Chapter 14
Low Temperature and Gravitation Wave Detectors

Fulvio Ricci

Abstract The success of a precision experiment is often associated to the use of low temperature techniques. In particular, when the thermal noise is a barrier for improving the experiment sensitivity, the cryogenics is crucial for beating this limitation. This strategy was applied in the case of the resonant gravitational wave detectors (GW) and now it is proposed for the future generation of the GW interferometers. In the following we summarize the history of GW detectors and we recall some of the basic principles of the cryogenic techniques. Then, we focus on the issues of cooling the mirrors of a GW interferometer.

14.1 Introduction

In the early 1960s, Joseph Weber initiated the experimental search for cosmic gravitational wave (GW) signals using massive aluminum cylinders with a fundamental longitudinal frequency of about 1 kHz and of a motion sensor converting the vibration of the bar into an electric signal [1].

In 1969, Weber announced the detection of signals in coincidence between two identical detectors set at a distance of nearly 1,000 miles [2]. The claim stimulated the construction and operation of new room temperature detectors, which gave no evidence that GW were being seen [3–6].[1] Despite of the controversial results, the scientific challenge of the direct detection of GW signals was launched and in 1970 William Fairbank at Stanford University proposed a new, much more sensitive

[1] Here we cite just few experiments among the several ones. A more detailed bibliography can be found in [7].

F. Ricci (✉)
Department of Physics, University of Rome La Sapienza and INFN Sezione di Roma,
Piazzale Aldo Moro 5, I-00185 Roma, Italy
e-mail: fulvio.ricci@roma1.infn.it

M. Bassan (ed.), *Advanced Interferometers and the Search for Gravitational Waves*,
Astrophysics and Space Science Library 404, DOI: 10.1007/978-3-319-03792-9_14,

detector, a five ton bar cooled to the mK range [8], which involve the use of cryogenics and superconducting techniques for noise reduction. W. Hamilton in Louisiana [9] and E. Amaldi and G. Pizzella in Rome [10] followed the same path starting to develop cryogenic detectors. The cryogenic antennas took data in coincidence more than two decade later and today two ultra cryogenic detectors that achieved a temperature of 0.1 K [11, 12], are in continuous data taking. Although we are still waiting for the first detection, these cryogenic systems improved by four order of magnitude the energy sensitivity over Weber's original antennas.

Since several years now, the sensitivities of the kilometer scale interferometers surpassed the sensitivity limits of the cryogenic bars [13], over a larger frequency band. At present we are upgrading the interferometer configuration and we expect (on the base of robust theoretical predictions) that these instruments in their advanced configuration will detect several GW events during the next quinquennium. In this scenario, even the study of a third-generation detector was started (see Chap. 13): it was focused on the realization of a GW observatory ten times more sensitive so that, at this level of sensitivity, it will turn the detection into a routine astronomical tool. The design study of the Einstein Telescope observatory (ET) has been recently completed, setting the specifications for the site infrastructure and the necessary technologies. Cryogenics is considered again one of the main technologies to be applied for beating the thermal noise limit achieved by the advanced detectors.

In addition, the construction of a new 3-km interferometer, KAGRA, has started in Japan: it is based on the use of cryogenics in an underground laboratory. Thus, the interest in all the aspects of the use of low temperature techniques for a GW detector is grown again.

The advantages of lowering the temperature T in a GW interferometer are summarized in the following list:

1. Test mass and suspension thermal noise are reduced at low temperature (see Chap. 8), being the displacement power spectrum of the mirror $S_{xx} \propto T$.
2. Thermoelastic noise in both the mirror substrates and in coatings decrease as T^2, because of the decrease of the thermal expansion coefficient.
3. The thermorefractive noise associated with the fluctuation of the refraction index decrease as T^2.
4. The acoustic losses of several materials characterized in terms of the loss angle Φ decrease at low temperature. Thus, the noise power spectral of the mirror displacement is expected to decrease as Φ.

Finally, we stress another important advantage: the thermal lensing is drastically reduced for two reasons:

1. Refraction index variation with temperature is very small at low temperature,
2. Generally, the thermal conductivity increases and consequently reduces thermal gradients on the mirror.

In Fig. 14.1, we show the expected sensitivity curves of the advanced detectors and a tentative curve of the ET sensitivity. The grey box indicates the spectral range where

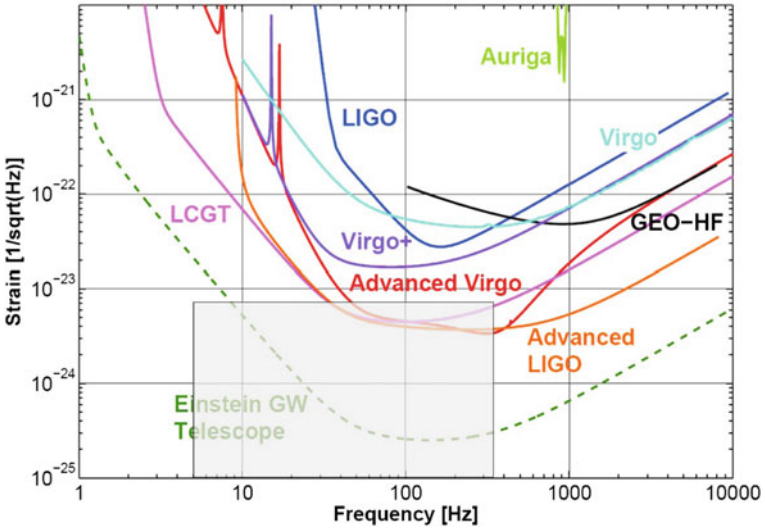

Fig. 14.1 Sensitivities of gravitational wave detectors from the first to the third generation. The *grey box* indicates the spectral range of the sensitivity dominated by the thermal noise

the dominant source noise is the thermal one. The main improvement is obtained by cooling the suspended mirror at low temperatures.

As we said before the use of low temperature for operating the GW detectors was proposed by W. Fairbank, who used to say...

Any experiment is better, if it is done at low temperature.

However, in case of a GW interferometer we are facing the challenge of cooling untouchable super-mirrors of more than 100 kg, suspended by thin crystal fibers in ultra high vacuum and in absence of any element polluting its surface. For this reason we also tend to agree with Bill Hamilton, who used to add to Fairbank's statement (Fig. 14.2):

Any experiment will be harder, if it is done at low temperature.

In the following sections, we introduce few fundamental concepts of cryogenics and then we discuss the main problem to be solved for cooling the super-mirrors of the ET detector without spoiling the stringent requirement of a GW interferometer.

14.2 Cryogenics

Research and development into the field of cryogenics began during the nineteenth century with the liquefaction of common gases as O_2 and N_2 (see Fig. 14.3). However, the great step forward, the storage of cryofluids, occurred in 1892 when sir James Dewar, a Scottish chemist and physicist, invented a double-walled container with a vacuum insulation flask. This was the crucial element that led the way to liquefy

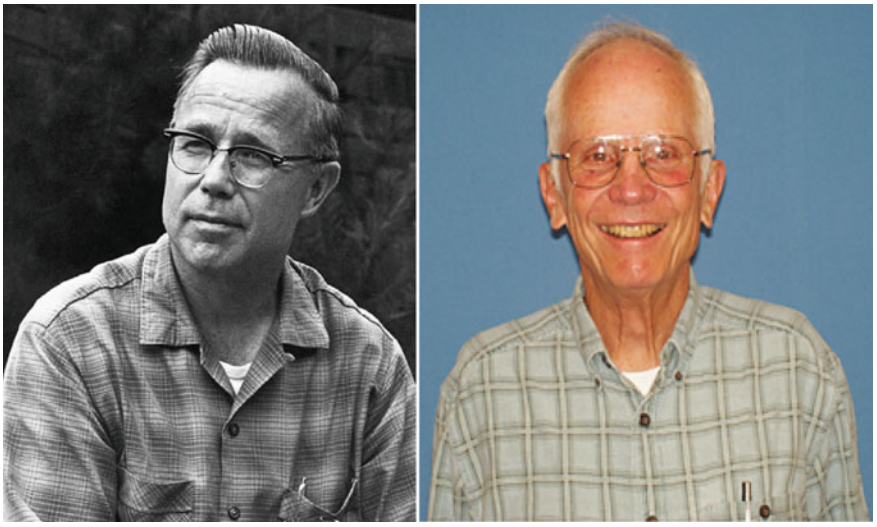

Fig. 14.2 On the left William Fairbank in the earlier 1970s. On the right William O. Hamilton these days

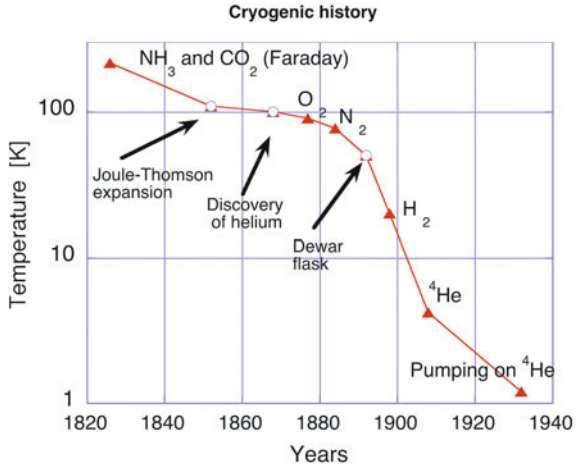

Fig. 14.3 Chronological development of the cryogenic techniques up to 1 K

helium, a liquid with an extremely low latent heat. Kamerlingh Onnes was able to attain the goal of the first successful liquefaction of helium in 1908. In the *old days* of low temperature physics, the production of liquid helium was a painful process. The experimentalist had to start in the early morning with liquid nitrogen ($T_{N_2} = 77$ K) to produce hydrogen ($T_{H_2} = 20$ K), by means of which it was possible to obtain at the end of the day the liquid helium ($T_{He} = 4.2$ K). Then, pushed by the need to produce liquid oxygen and hydrogen used as propellants for missiles, in the 1940s

commercial development of gas liquefiers began. Samuel Collins designed a machine providing helium without the need to liquefy hydrogen and even without nitrogen. Today nitrogen and helium cryogenics has progressed and a variety of liquefiers exist for small or large liquid helium production.

Cryogenics has many applications. Cryogenic liquids, such as oxygen, nitrogen, and argon, are often used in industrial and medical applications. Taking advantage of the reduction with temperature of the vapor tension of gas, the cryogenics is used for producing high vacuum. Other applications include fast freezing of some foods and the preservation of biological materials such as human blood, tissue, and embryos. Moreover, the electrical resistance of most metals decreases as temperature decreases. Certain metals lose all electrical resistance below some transition temperature and become superconductors. An electromagnet wound with a wire of such a metal can produce extremely high magnetic fields with no generation of heat and no consumption of electric power once the field is established and the metal remains cold. These metals, typically niobium and titanium alloys cooled to 4.2 K, are used for the magnets of magnetic resonance imaging (MRI) systems in most hospitals. The industrial application of cryogenics can be synthesized in various categories of applications

1. Storage of gases
2. Vacuum systems
3. Low noise detectors and superconductors
4. Biological and medical applications.

Cryogenic fluids are also used in a variety of applications for research. Among the large-scale applications of cryogenics, the most impressive is by far the cryogenic plant set for the Large Hadron Collider at CERN, a proton-proton accelerator fully equipped with cryogenic magnets cooled at 1.9 K along the entire particle ring 27 km long.

In the case of small-scale applications of cryogenics, more and more often the use of cryogenic refrigerators (cryocoolers) is preferred to cryofluids. Cryocoolers are required for a wide variety of applications, and the number of applications keeps expanding as improvements to cryocoolers technology are achieved. One of the earliest applications, appeared about 50 years ago, was for cooling infrared sensors to about 80 K for night vision capability of the military. Then, they have been in widespread use for tactical military applications to meet ground, airborne, and shipboard infrared sensor cooling needs. Today the list of targeted applications is impressively broad: it includes IR detectors, low noise amplifiers, front-end passives in communication systems, SQUIDs, MEMs and next generation nanoscale devices.

While there are several types of cryocoolers, most operate on some variation of a common process. Gas is circulated through a closed cycle to absorb heat from the interior of the device and transfer it to the outside environment. This gas may be helium or some other mixture of gases. The ability of the device to cool its interior environment depends largely on the thermodynamic properties of the gas circulating through the system. Cooling cycles in these devices begin with gas being sent to a

compressor. As the compressed gas passes through a heat exchanger, it absorbs heat from the cryocooler, thereby cooling anything connected to it. When this gas absorbs heat at a constant volume in the heat exchanger, its pressure increases. It expands in volume and its pressure decreases in the next portion of the cycle. Finally, it returns to the compressor, which completes a closed loop through the cycle, and begins to circulate through the cycle again.

Common types of cryocoolers include the Joule–Thomson cooler, the Gifford-McMahon and the Stirling cooler, the pulse tube (PT) refrigerator, etc. Although less efficient than other devices, Joule–Thomson cryocoolers provide advantages in reliability and low electrical and mechanical noise levels,[2] while the more efficient coolers generate vibration due to the piston movement in the cold environment.

In the case of the mirror cooling for a GW interferometer we will analyze both methods to bring the mirror at low temperature, i.e.,

1. the first is based on the use of cryofluids
2. the second method relies on a battery of PT cryocoolers, which are more efficient than the Joule–Thomson systems and weaker source of mechanical noise than the traditional McMahon or Stirling machines.

14.2.1 The Cryofluids

The simplest way to produce low temperature is still the use of cryoliquids (e.g., nitrogen, helium). Liquid oxygen and hydrogen are rarely used in refrigeration: the former because of its high chemical reactivity, the latter again for its flammability. Both cryoliquids find also important applications in the space activity and in the industry. In the following table, we summarize some of the thermodynamical properties of cryofluids.

For our purpose, helium is the most interesting element and the most used in cryogenics after nitrogen. There exist two stable isotopes of helium, both of strong cryogenic interest (Table 14.1):

1. ^{4}He(nuclear spin $I = 0$). The ^{4}He content of near-surface atmospheric air has been determined to be 5.2204 ± 0.0041 parts per million by volume. To get it for industrial use ^{4}He is found in the natural gas field (mainly in Russia and the USA) with a concentration of $\sim$7 %.
2. ^{3}He (nuclear spin $I = \frac{1}{2}$). The ^{3}He/^{4}He ratio for atmospheric helium is established as 1.393×10^{-6}. By far the most common source of ^{3}He is the nuclear weapons program, of which it is a byproduct. In fact, the nuclear weapons program produces tritium which decays into helium-3.[3]

[2] The Joule–Thomson cryocoolers are based on an adiabatic expansion of the gas through an impedance orifice or a valve. This procedure is called a throttling process, and it permits to cool the gas when it is kept below its inversion temperature.

[3] During the cold war, the USA, Russia, and other countries stockpiled tens of thousands of nuclear weapons, and in doing so accumulated vast amounts of ^{3}He. Initially, the National Nuclear Security

Table 14.1 Thermodynamical properties of the two helium isotopes

Properties	^{3}He	^{4}He
Density [g/cm^3] (T = 0 K)	0.0863	0.146
Boiling temperature T_b (K)	3.191	4.215
Critical temperature T_c (K)	3.324	5.20
Critical pressure (bar)	1.165	2.289
Critical density (g/cm^3)	0.0413	0.0693
Melting pressure (T = 0 K) (bar)	29.31	25.32
Maximum superfluid transition temperature (K)	0.0025	2.177
(Gas at 300 K and 1 bar)/(Liquid at 1K) volume ratio	662	866

^{4}He plays a crucial role for achieving temperatures down to ∼1 K. Below it ^{3}He or a mixture of both liquids is used.

Liquid helium is notoriously difficult to handle. If you do not use the correct equipment or techniques, you can easily lose all the liquid, because of the very low latent heat of vaporization. For example, a heat load of 1 W will evaporate 1.41 of liquid per hour. Moreover, we have to stress that the latent heat of evaporation L_{ev} and the vapor pressure p_{vap} are fundamental parameters when using a cryo-liquid in the refrigeration process. The evaporation process provides a refrigeration power W_{ev}, which depends on L_{ev} and p_{vap}. However, looking at Table 14.2, we note that the value $L_{ev} = 2.56$ kJ/l for ^{4}He is very small in comparison, for example, with that of hydrogen (31.8 kJ/l) or of nitrogen (160 kJ/l). A low value of L_{ev} means a small cooling power, a serious drawback when cooling by evaporation. To increase the refrigeration efficiency of the cooling process, the enthalpy of the cold gas warming from 4.2 K to room temperature is used. The curve of the ^{4}He enthalpy versus temperature is shown in Fig. 14.4.

For example, on the cooling process of a 100 g of Cu, the full use of the ^{4}He enthalpy reduces at just 0.08 l the amount of the liquid helium, i.e., 1/30 times the amount needed using the ^{4}He latent heat only. In practice, if the material is cooled by cold helium gas flowing over it, the amount of liquid helium is reduced by a following theoretical factors:

1. 32 in the range 300–4.2 K
2. 10 in the range 77–4.2 K

When the liquid helium-4 and its vapor are cooled to 2.177 K, known as its λ point, a third phase forms still liquid. The new liquid *He-II* showsthe remarkable

(Footnote 3 continued)
Administration (NNSA) and its predecessor agencies, which have maintained the US tritium stockpile, used to consider the gas useless and they considered to vent it into the atmosphere. In the 1980s, however, scientists began to realize the potential of ^{3}He as a neutron detector and the price skyrocketed.

Table 14.2 Boiling and melting temperature at 1 bar of gas and their latent heat

Substance	T_b Boiling temperature at 1 bar (K)	T_m Melting temperature at 1 bar (K)	Latent heat at T_b L_{ev} (kJ/l)
H_2O	373.15	273.15	2252
NH_3	293.8	195	–
CO_2	194.6	216	–
Xe	165.1	161.3	303
Kr	119.9	115.8	279
CH_4	111.18	90.8	–
O_2	90.2	54.4	245
Ar	87.3	83.8	224
N_2	77.4	63.3	160
H_2	20.3	14	31.8
^{4}He	4.21	–	2.56
^{4}He	3.19	–	0.48

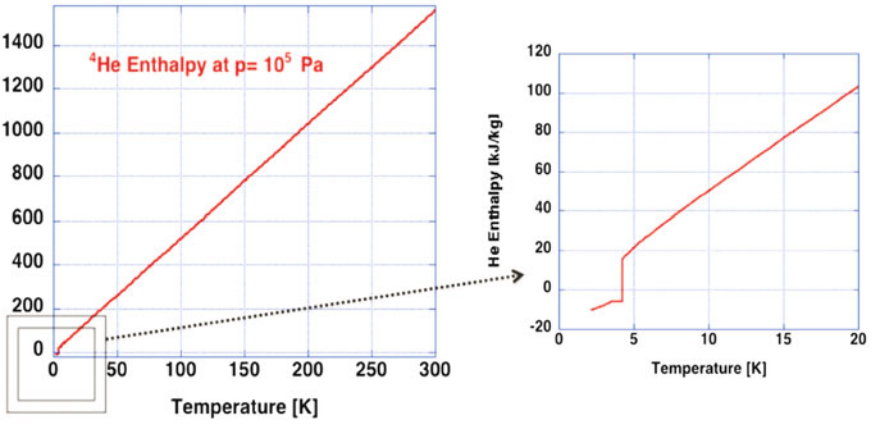

Fig. 14.4 The enthalpy of the ^{4}He gas in the range 2–300 K

property known as superfluidity.[4] It flows with practically no friction through small openings and narrow capillaries and if we plot the volume rate flowing in a capillary versus temperature we note the striking change in the curve slope crossing the λ point. The flow of helium II acts as if it were a mixture of two fluids [14–17]. One, called the superfluid, has no viscosity or entropy and can flow without dissipation through extremely narrow channels. The other, called the normal fluid, does have a finite viscosity and carries all the entropy. The liquid is pictured to be all normal fluid at the lambda transition and all superfluid at absolute zero.

Above the λ-point, ^{4}He shows transport properties similar to those of a classic fluid; it has a low thermal conductivity (a factor of 10^{-4} compared to Cu and a factor

[4] The liquid phase above the λ point is named *He-I*.

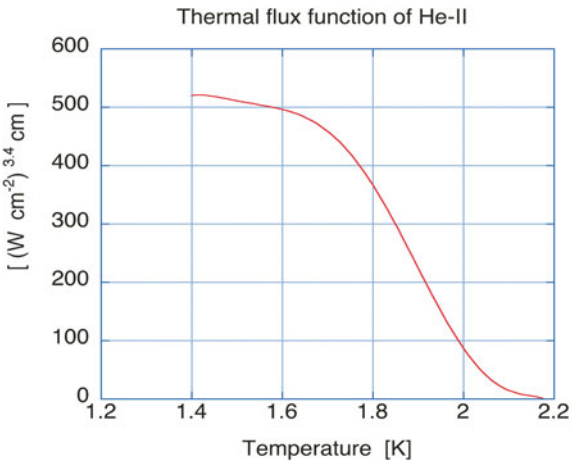

Fig. 14.5 Thermal flux function of the liquid helium $\dot{Q}^n L$ below 2.2 K versus temperature

of 10^{-1} compared to stainless steel) and boils with strong bubbling. In particular, when pumping on *He-I*, bubbles of vapor form inside the liquid, which is warmer than the surface cooled by the evaporation process.

Below 2.17 K, the properties of heat conduction in the liquid helium drastically change. The steady-state heat flux $\dot{Q}$ in a tubular conduit of length L, the ends of which are maintained at temperatures T and T_w, is expressed by the empirical relation

$$\dot{Q}^n = \frac{X(T) - X(T_w)}{L} \tag{14.1}$$

where $n = 3.4$ is the exponent value derived from the best experimental fit, and $X(T)$ is a function of temperature shown in the Fig. 14.5, physically analogue to a conductivity integral [18]. On the base of this information, it is possible to show that the highest heat flux per unit temperature is maximized near 1.9 K.

As an example, the heat flux transported by conduction between 1.9 and 1.8 K in a helium tube one meter long is $\sim 1.2\,\mathrm{Wcm}^{-2}$, which corresponds to a specific heat flux per unit surface three orders of magnitude higher than that through a similar bar made of OFHC copper. Because of the very high thermal conductivity, the temperature gradient in the *He-II* bath is very close to zero, and for this reason ***bubbles do not form in the liquid*** during the evaporation process.[5]

The absence of boiling in *He-II* is a great advantage in a GW cryogenic detector. In fact, the long history of the cryogenic GW experiments can be told as a never ending fight for reducing the residual vibration associated to the boiling of the cryofluids. We just recall here the case of the Explorer antenna installed at CERN [19]. In the plot we show in the vertical axis the detector output filtered for enhancing the sensitivity

[5] The high thermal conductivity allows also for the propagation of temperature waves (called *second sound*), which are reflected and diffracted as standard waves, but which give rise to temperature variations in small regions.

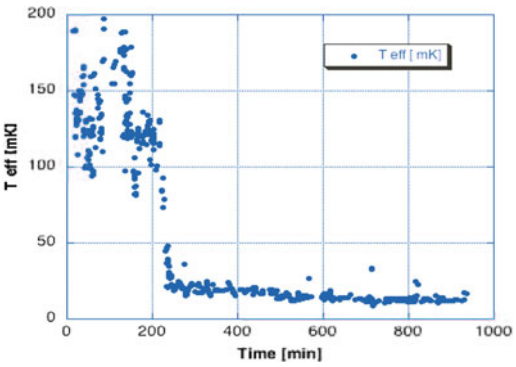

Fig. 14.6 The output of the GW detector Explorer when we were pumping on the ^{4}He bath. The sharp change is in coincidence of the λ point crossing

to the sudden change of the vibration energy of the detector. On the horizontal axis, we show the time referred to a period during which we were pumping on the liquid helium bath of ∼3000 l and decreasing its temperature from 4 K down to 1.5 K. In Fig. 14.6, we notice the striking reduction of the detector output observed during and after the λ point transition, when the boiling noise disappeared.

Noise associated with the boiling of the cryofluids was experienced by other resonant GW detectors and it can be also a potential problem for the third generation of GW interferometers. In fact, some disturbances associated to the boling process of cryofluids has been observed already during the refilling phase of the N_2 cryotraps mounted both in LIGO and VIRGO.

In a design phase of the detector, there is the need to quantify the effect of the boiling on the GW test masses. Our need is to infer the acceleration (or displacement) noise induced on the wall of the test mass container. The noise spectral density of the acceleration due to the boiling process depends on the boiling rate and on the geometry and the material of the container. For example, in the case of the GW resonant antenna Explorer, we evaluated the order of magnitude of the random displacement of the wall of the helium container, a stanley steel cylinder of ∼1.6 m diameter and ∼4 m long. The r.ms. value of the displacement noise, peaked around 900 Hz, was of the order of 10^{-10} m at 4 K when the boiling rate of the liquid helium was ∼2 l/h.

Since the power spectrum of the boiling noise is mainly concentrated in the acoustic range, it can be measured using sound level meters (see Fig. 14.7). The signal output of these microphones, proportional to the pressure change detected on the microphone surface, is calibrated to give the relative sound intensity I_r in $\mathrm{dB_{SPL}}$ units:

$$I_r\ [\mathrm{dB_{SPL}}] = 10 \times \log(I/H),$$

where I is the sound intensity (usually measured in $\mathrm{W/m^2}$) and $H = 1.0 \times 10^{-12}\ \mathrm{W/m^2}$. The quantity H is an intensity reference value corresponding to the earing threshold of a normal ear in good health. This should correspond to a hear

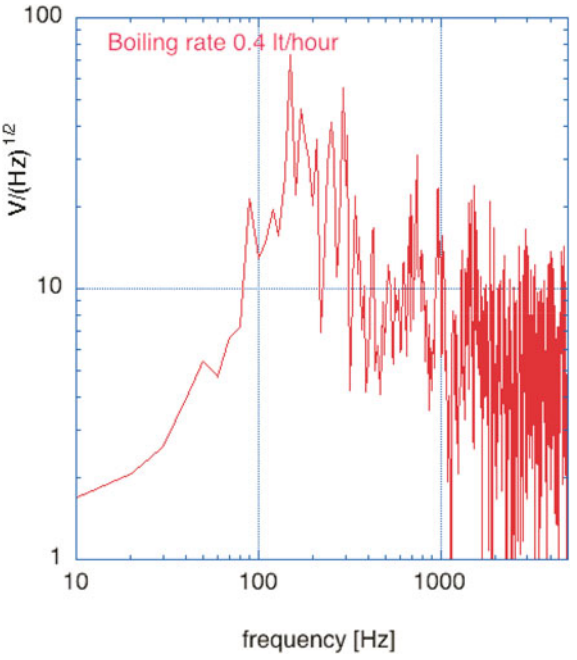

Fig. 14.7 Pressure noise spectrum of a boiling fluid in a cylindric container of 10 cm diameter and 30 cm height, made of steel. The boiling rate was ∼0.4 l/h. In the *vertical axis* we show the spectral density of the amplified output voltage of the microphone and on the x-axis the frequency. The voltage/pressure factor was 6.3×10^{-2} Pa/V

pressure change $\Delta p_0 = 20\,\mu$Pa. Under this assumption, the microphone noise can be translated also in terms of a pressure change being

$$L_{\mathrm{SPL}} = 10 \times \log(I/H) = 20 \times \log(\Delta p_1/\Delta p_0).$$

Then, the pressure fluctuation is interpreted as a stress field applied to the walls of the test mass container, provided that a correction factor, which takes into the account the distance and directionality of the microphones with respect to the container wall, is included.

Unfortunately this is not the end of the story. The companies producing audio systems calibrate often their devices in dBA units. To give an idea of the sound level in dBA, we report here a couple of common cases:

- a whispering level of noise is ranging around 20 dBA, which corresponds to $\sim 2 \times 10^{-4}$ Pa,
- a bird twitter outside at 15 m distance is quoted around 50 dBA corresponding to $\sim 6.3 \times 10^{-3}$ Pa.

The letter *A* following the abbreviation dB designate a frequency-response function that filters the sounds picked up by the sound level meter. The filter shape is not standard and it can change from microphone producer to producer. The consequence is that there is not a conversion formula for measured dBA values to sound level in

dB_{SPL} or vice versa and the lesson is that often this kind of measurements gives just the order of magnitude of the acoustic disturbance.

In practice, the most reliable approach for inferring the sound noise contribution to the noise budget of a GW detector is to put in contact with the container wall a full set of low temperature accelerometers, which monitor the random movement induced by the boiling (Fig. 14.7).

The quietest scheme for cooling the test mass of a GW detector is the *Claudet bain*: it permits to use super fluid helium at atmospheric pressure and to insure continuous refilling from the container of the helium in the normal state

A ^{4}He bath at 4 K at atmospheric pressure flows gently through a high impedance porous filter acting also as acoustic filter to a second ^{4}He bath kept in thermal contact with a cell unit cooled below the 2 K. In this way, the *He-II* bath is in a quiet hydrodynamic status well far from the boiling point and with enhanced heat removal capability. Moreover, since *He-II* is modeled as a mixture of two fluids flowing with velocities of opposite sign (the superfluid and the normal component), it should be possible to operate the cryo system in the state of zero mass flow [20]. This implies that, in absence of the vapor phase, we have

$$\rho_s v_s = -\rho_n v_n \tag{14.2}$$

where ρ and v are the density and the velocity of the normal (n) and superfluid (s) components.

In this condition, in principle the test mass can be in a direct thermal contact with a cold element filled by superfluid helium at atmospheric pressure. However, the fluid still transmits sound waves and we should limit the acoustic effect of the cooling fluid on the test masses. Therefore, this approach requires also a deeper analysis of the impact of the acoustic losses of the fluid to the dynamic behavior of the suspended test masses [21].

In conclusion, as we will discuss later, the simpler and safer approach will be to fill a copper box with He-II at atmospheric pressure and bring the refrigeration power to the mirror through its suspension wire made of a crystalline material.

14.2.2 The Cryocooler

The vapor-compression refrigerator, first developed in the latter part of the nineteenth century, in a single stage produced temperatures down to about 230 K. Since the middle of the twentieth century a steadily increasing demand for cryogenic temperatures below 120 K has developed for a wide variety of applications. Initially most of these applications required to develop very large plants with power inputs of many megawatts. Then, a need for small cryogenic refrigerators (cryocoolers) has evolved triggering an impressive research and development effort during the past 40 years (see Fig. 14.8). One such cryocooler, the pulse tube (PT) refrigerator, first conceived in the mid-1960s, was of academic interest until the mid-1980s. At the Moscow

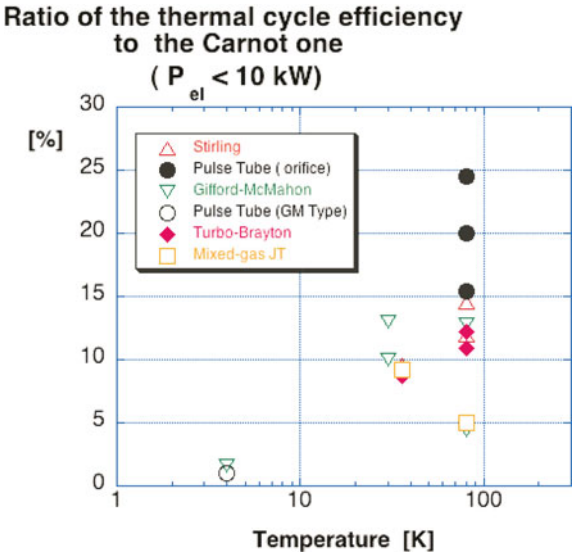

Fig. 14.8 Ratio between the thermal cycle efficiency of refrigeration and the corresponding Carnot cycle efficiency versus temperature

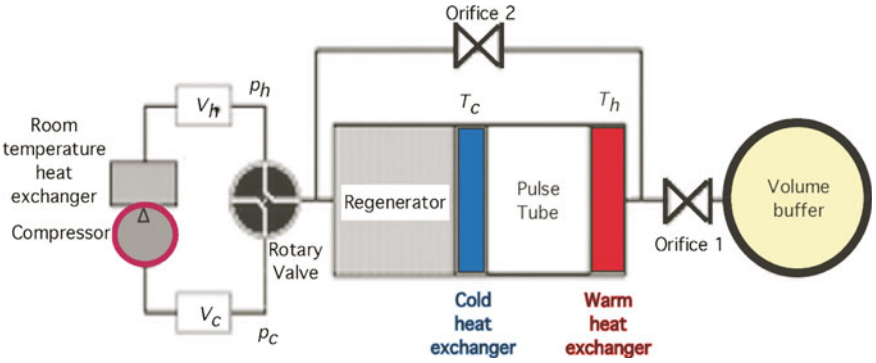

Fig. 14.9 Scheme of a pulse tube cryocooler

Bauman Technical Institute in 1984 Alexander Mikulin et al. [22] introduced an orifice inside the pulse tube near the warm end and achieved a low temperature of 105 K. Since then, improvements in its efficiency have occurred rapidly.

Unlike the Stirling or Gifford-McMahon refrigerators, the PT one has no moving parts at the cold end (see Fig. 14.9). Therefore, no expensive high-precision seals are required and the cold head can be operated without any service inspection. In this way, some of the problems associated with cryocoolers in many different applications, such as vibration and reliability are attenuated (Table 14.3).

Subsequent modifications and improved designs yielded much improved efficiencies.

Table 14.3 Progress of the pulse tube technology

Year	PT type	Final temperature (K)	P_{cool} (W)	P_{el} (W)
1993	Single stage	80	0.8	33
1994	Single stage	77	133	3400
1995	Double stage	4.2	0.5	6300
2004	2 double stages for ^4He and ^3He	1.3	0.04 (@2 K)	4500+1300

P_{cool} is the refrigeration, P_{el} the electric power of the compressor

Pushed in large part by NASA and the military, the efficiency figures, i.e., the ratio P_{cool}/P_{el} are still improving, thanks to the effort of the research laboratories and few commercial companies.

The Pulse Tube cryocooler (PT) is based on the displacement and the expansion of a gas, usually He^4. The working fluid undergoes an oscillating flow and an oscillating pressure. A typical average pressure in a PT is 25 bar, and a typical pressure amplitude range between 2 and 7 bar.

A piston compressor and a set of switching valves are used to create the pressure oscillations of the helium gas. A crucial element of the cryocooler is the PT regenerator. It is a heat exchanger, which acts as cold storage systems for the pulsed flow processes used in the cryocooler.

The piston moves periodically pushing the gas, which enters the regenerator with temperature T_h and leaves it at the cold end with temperature T_c, hence heat is transferred into the regenerator material. On its return the heat stored within the regenerator is transferred back to the gas.

In practice, the regenerator stores the energy from one stream and later transfer the energy to a second stream, for example between the out-of-phase pulses of gas.

Let us consider a gas element entering the tube with temperature T_h and leaving it with a higher temperature when the pressure in the tube is low. Later in the cycle the same element is pushed out the tube again when the pressure inside the tube is high. As a consequence, its temperature will be higher than T_h. In the heat exchanger, it releases heat and cools to the ambient temperature T_h. At the cold end of the pulse tube, there is the opposite effect: here gas elements enter the tube when the pressure is high with temperature T_c and return when the pressure is low with a temperature below T_c. The heat is extracted from the cold point, providing the desired cooling power.

The thermal environment of a gas element, that moves back and forth in the system, changes when it passes the heat exchanger. In the regenerator and in the heat exchanger, the heat contact between the gas and its surrounding material is good. Here the temperature of the gas is practically the same as that of the surrounding medium. However, in the pulse tube the gas element is thermally isolated, so, in the pulse tube, the temperature of the gas element varies with the pressure.

As we said before, Mikulin and his co-workers [22] inserted a flow resistance (the orifice) at the warm end of the pulse tube to allow some gas to pass to a large reservoir acting as buffer volume. This is typically 10 times larger than the volume

of the pulse tube and its pressure is almost constant and close to the average pressure in the pulse tube. The combination of the orifice and the buffer provides a phase difference between the flow of the gas in the tube and the pressure oscillation; such phase difference is necessary for the performance of the PT.

In 1990, Zhu et al. [23] connected the warm end of the pulse tube with the main gas inlet by a tube, containing a second orifice. Thus, a part of the gas could enter the pulse tube from the warm end, bypassing the regenerator. The function of the second orifice is to reduce losses. It allows some gas to bypass the regenerator and to enter the pulse tube directly.

The quality of the regenerator material sets in practice the cryocooler performance. It consists of a porous matrix of finely divided material in the form of wire mesh, plates, or small balls. These forms maximize the surface area and minimize the thermal conduction necessary within the solid to maximize the heat transfer with the surrounding gas within the duration of a cooling cycle. The regenerator stores the heat of the gas during a half-cycle and, therefore, it must have a high heat capacity, compared to the heat capacity of the gas.

At temperatures above 10 K materials as bronze or stainless steel are often used. Below 10 K one uses rare earth materials, which are specially developed for this application.

To obtain temperatures below 20 K, the system is operated at low frequency ($\nu \sim 1$ Hz). The frequency defines the diffusion depth δ in the working gas and the regenerator material:

$$\delta = \sqrt{\frac{k}{\pi \nu C}} \tag{14.3}$$

where k is the heat conductivity, ν is the frequency and C is the volumetric heat capacity of the regenerator material. It follows that when the frequency is increased, the diffusion depth decreases, and the heat storage in the regenerator degrades. Moreover, a high operating frequency leads to a large pressure drop in the regenerator, i.e., a poor performance of the system.

A pulse tube cryocooler seems to be suitable for cooling the mirrors of the GW interferometer. However, also this kind of refrigeration system injects mechanical noise because of the gas pulse flowing in its cold head.

We measured the acceleration of the 4 K cold head of the Pulse Tube 407 of CRYOMECH and that of the Sumitomo SRP-052A (see Fig. 14.10).

It results that the noise produced by this kind of refrigerators is still too high for cooling the GW test masses so that it is necessary to design a cooling system, which can attenuate the PT cryocooler vibrations. An active system to reduce the residual vibrations associated to the gas pulse is the so-called Vibration Free Cryostat (VFC) cryostat [24]: it was conceived to host a suspended mirror cooled by a PT cryocooler.

The cryostat scheme is sketched in Fig. 14.11. It is based on the idea to attenuate the cryocooler vibrations by directly acting on it and consequently allowing a shorter heat link between the cryocooler and the mirror.

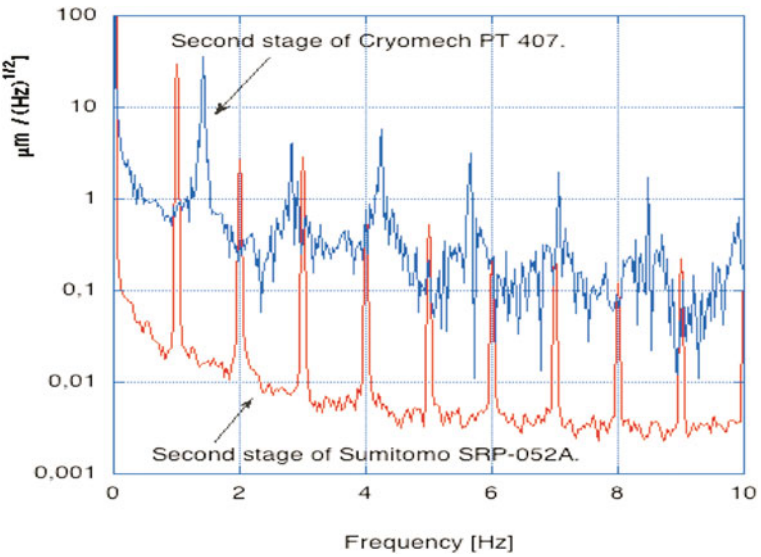

Fig. 14.10 We show the displacement noise spectrum of the coldest point of the CRYOMECH PT407 obtained by by an accelerometer for low temperature applications. The similar data taken on Sumitomo SRP-052A are obtained using an optic fiber sensor

The active control on the cold head vibration is performed by a digital feedback system in which the cold head displacement are monitored by a low temperature sensor. The sensor output provides the error signal for the correction, which is performed at room temperature by piezoelectric actuators.

The cryocooler cold head is clamped to a platform placed on dampers and it is connected to the cryostat by means of an elastic bellow designed to mechanically decouple the head and the platform from the lower part of the cryostat connected to the ground. The feedback correction signal is sent to three piezo-actuators which are loaded by the platform and can act on it from below. The attenuation provided by this system is of the order of 200. Then, in a GW detector, the cold head will be connected to the test mass via flexible heat links insuring an other signifiant insulation factor.

However, for achieving the ET sensitivity goal a R&D activity on a further reduction of the PT vibration is highly recommended. The pulsed force due to the gas deforms the tube of the cold head displacing the cold plate of several micrometers. This effect has been simulated via finite element software showing that, depending on the the cold head geometry, the longitudinal expansion of the tube can be of the same order the horizontal displacement. Thus, there is still a large margin of improvement changing the geometry of the cold head and/or enhancing both the active and passive attenuation damping of the gas pulse effects.

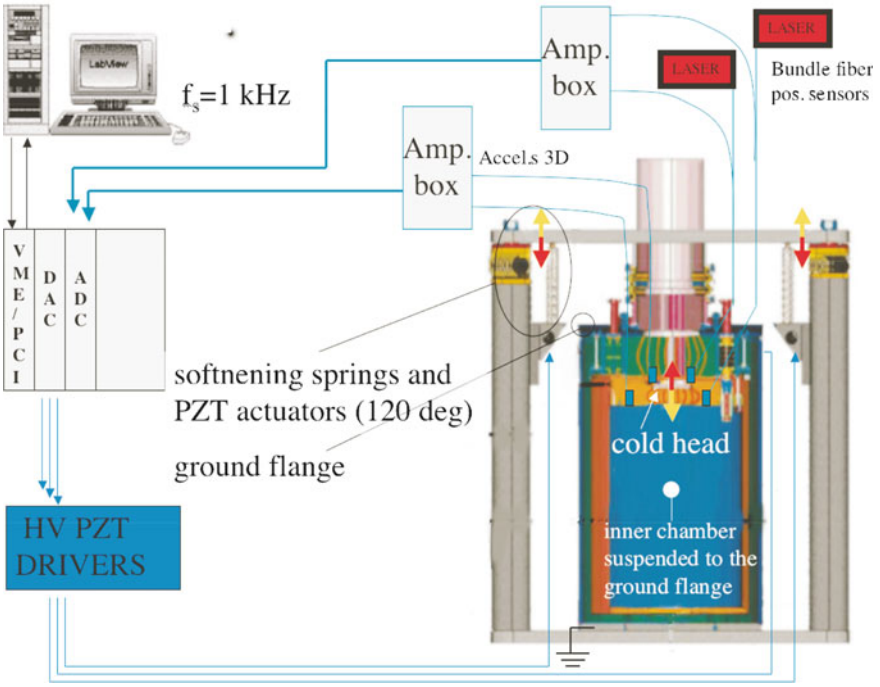

Fig. 14.11 Sketch of the vibration free cryostat

14.2.3 Cooling Strategy Comparison

The two methods for cooling the mirrors have both advantages and drawbacks. The cryocoolers insure a longer duty cycle for the GW observatory and they require less maintenance and manpower.

Moreover, the use of cryocoolers in an underground environment significantly relaxes all the safety issues associated with the use of cryofluids in an ambient with limited ventilation.

On the other hand, the main limitations of this approach are

- the low refrigeration power that implies the use of a battery of cryocoolers and associated compressors to be installed in the underground laboratory not too far from the test masses,
- the low efficiency, which requires a large amount of electric power to be distributed in the laboratory,
- the residual vibrations of the cold heads and the acoustic noise transmitted along the high pressure helium gas lines.

The use of cryofluids implies the construction of a cryoplant outside the underground laboratory surface: it will be the production center of liquid helium hosting

the liquefiers and the compressors. Then, the liquid helium will be transferred to the cryostats using special low loss lines deployed from the surface to the underground interferometer. This system has a higher cost, needs more manpower and more stringent safety requirements.

The KAGRA project has already chosen the cooling strategy based on PT: they are confident that at the level of sensitivity of the advanced detectors it is possible, with present technology, to damp enough of the residual vibration of the cryocoolers. The entire GW community will follow their experience, which will orient also the final technical design of the Einstein Telescope detector.

14.3 The Cryogenic Payload

The last suspension stage, simply called the *payload*, is suspended from a long series of pendula kept at room temperature, for reducing the seismic and acoustic disturbances (the super attenuator). The payload is designed to compensate the residual seismic noise and to steer the mirror through internal forces exerted from the last element of the super attenuator. The main components of the payload are: the Marionette, the Recoil Mass, and the Mirror (see Chap. 7). The marionette is the first stage used to control the mirror position by means of coil-magnet actuators acting between the last stage upper part suspension and the marionette arms. The recoil mass[6] is used to protect and to steer the mirror by means of the coils of the electromagnetic actuators acting on four small magnets mounted on the mirror back side.

The mechanical losses of the suspended mirror determine the thermal noise contribution of interferometer sensitivity because of the well-known relation between mechanical dissipations and thermal motion in macroscopic systems (see Chap. 8). The parts in contact with the mirror are made of materials having intrinsic low mechanical dissipation; in particular, the suspension wires are attached by means of low friction mechanical clamps. Cryogenic operation introduces additional difficulties, but the benefit in thermal noise reduction can be enhanced by the selection of materials with improved properties at low temperatures. Moreover, to take advantage of the low temperature, the design of a last stage suspension should satisfy a couple of new requirements in addition to those of a room temperature payload:

1. the refrigerating power transmission to the mirror level should not deteriorate the position control performance;
2. the residual vibration transmitted to the mirror through the cryogenic system, should be well below the detector noise sensitivity curve.

As a consequence, a good mechanical isolation between the mirror and the cooler is necessary. Another important element in a cryogenic system is the thermal link

[6] The idea of using a reaction mass to control a suspended mirror has been originally pursued by the GEO group [25].

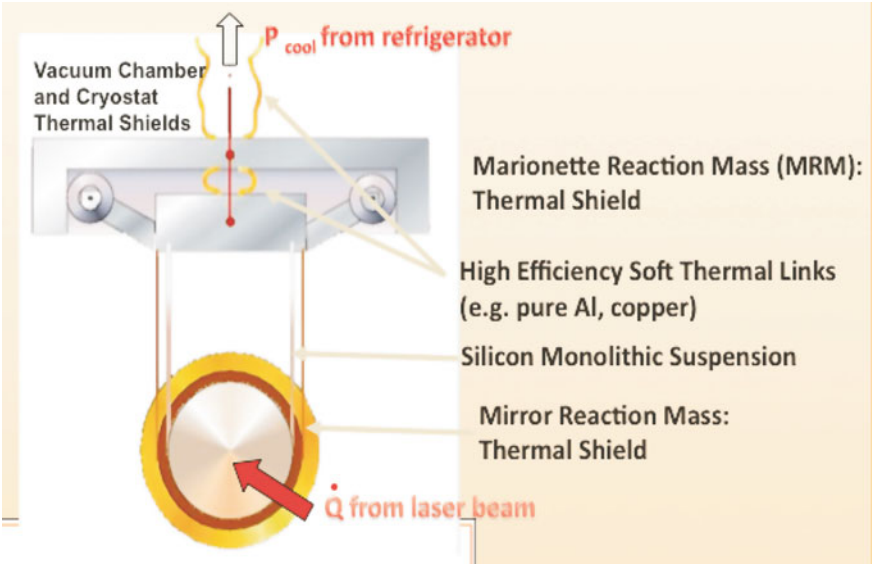

Fig. 14.12 Scheme of the cryogenic payload

with the refrigerator. Taking care of having short thermal links and good thermal couplings is important to have low refrigerating power losses. For instance, the use of a mechanical attenuator as a heat link is a good solution to damp the vibrations of the cooler, but has the disadvantage to limit the heat flow. On the other hand, the mirror suspension itself must have the required thermal conductivity to reduce thermal gradients and to optimize the cooling time.

The requirements we have just described suggest that the new system will be the result of a trade-off between the need to have a strong thermal contact with the refrigeration apparatus and the need to reduce any dissipation source due to the coupling of the suspension with the mirror. Thus, the materials used for building a cryogenic payload must have high thermal conductivity as well as good mechanical and optical properties at low temperature. Crystalline materials are preferred at low temperature for their thermal capacitance properties and in particular sapphire and silicon appears to be the best candidates, both for the mirror and for its suspensions. Indeed they have high thermal conductivity, low thermal expansion rate and very low mechanical losses at cryogenic temperatures. If test masses of large size are required, as in the ET case, then silicon is preferred.

In the Fig. 14.12 of the payload scheme, it is shown how a cryogenic suspension should work during the interferometer operation, i.e., when the payload has been cooled down and the laser is turned on. The fraction of the laser power, which is absorbed by the mirror ($\dot{Q}_{\text{laser}}$), flows through suspension wires; then it crosses the points where the suspension wire clamps are set and reaches the refrigerating system.

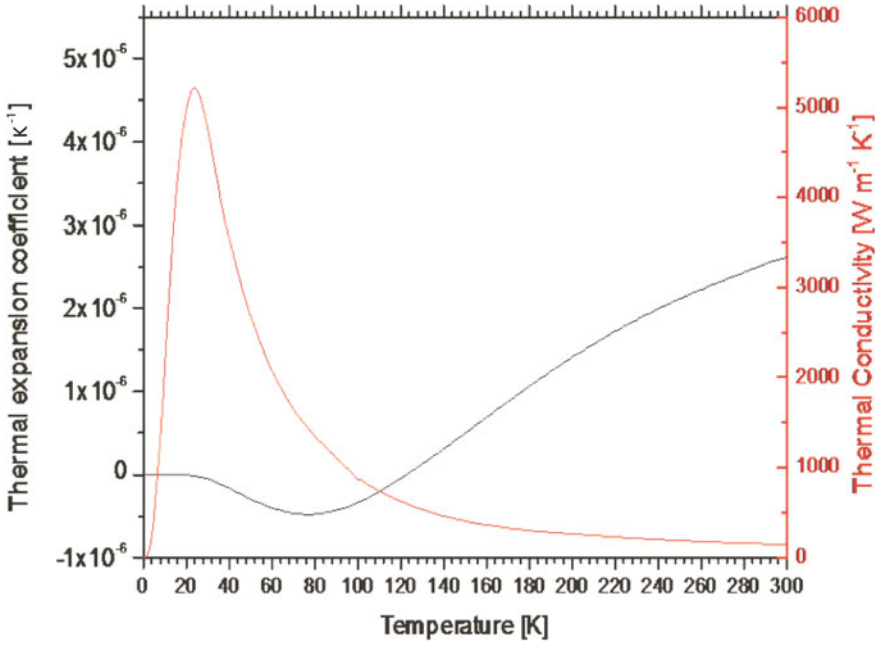

Fig. 14.13 Thermal properties of silicon. The *red curve* represents the thermal conductivity, the *black one* the thermal expansion coefficient, a crucial properties of the material for reducing the thermal lensing effect in the optical element

To this aim, the marionette has to be connected with very efficient, soft heat links to the cooling power.

In a similar way as for the mirror, the reaction mass is cooled down via its suspension wires and, if there is not extra thermal input, it reaches the thermal equilibrium and acts as a thermal shield for the mirror. The choice of the wires for the recoil mass must fulfill the request of having a good mechanical and thermal performance. For this reason, the use of a silicon suspension also for this part is the most obvious option (Fig. 14.13).

14.3.1 Payload Thermal Input and Heat Extraction

The main heat inputs into the cold mirror of the interferometer are the thermal radiation coming from the warm surface of the kilometric vacuum tube hosting the laser beam of the interferometer. To this, we have to add it the heat load due to the absorption of a small fraction of the laser light by the mirror surface (see Fig. 14.14). The latter is estimated considering that the laser power circulating in the optical resonant cavity of the interferometer. For example, let us assume 1 ppm

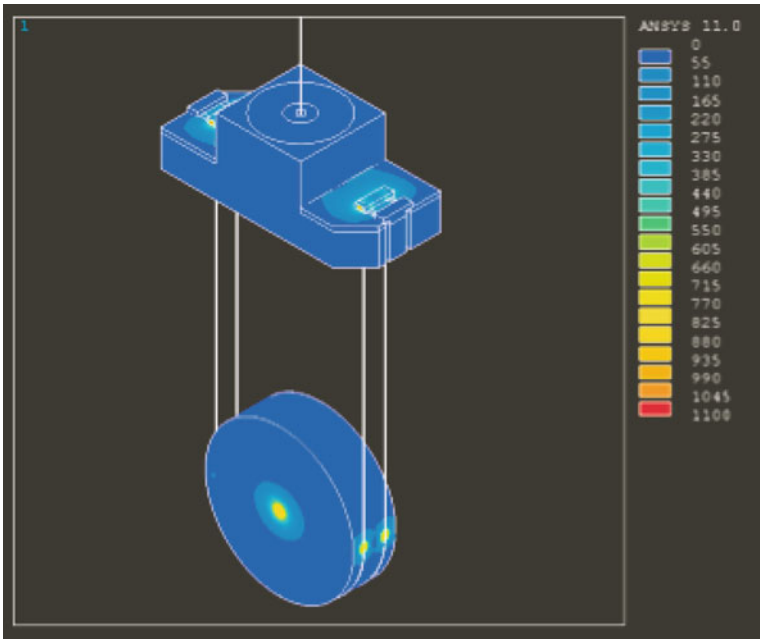

Fig. 14.14 Finite element analysis of the heat flow from the mirror to the marionette via the suspension wires, when the laser is impinging on the mirror

as a reference value for the absorption coefficient of the mirror optical coating at the laser wavelength. In this case, if ∼20 kW of light power are stored in the interferometer, we have ∼20 mW of absorbed laser power.

The radiation from the warm surface of the vacuum tube to the mirror is derived from the Stefan-Boltzmann equation and we have:

$$\dot{Q}_r/A_1 = \sigma F_e F_{1-2}(T_2^4 - T_1^4) \tag{14.4}$$

where $\dot{Q}_r/A_1$ is the heat transfer rate by radiation per unit area of the mirror surface, $\sigma = 5.67\,10^{-8}\,\mathrm{W/m^2/K^4}$ is the Stefan-Boltzmann constant, F_e is the emissivity factor, and F_{1-2} is a geometric configuration factor relating the two surfaces, whose temperatures are T_2 (warm) and T_1 (cold). From Eq. 14.4 the heat flux on the mirror at $T_1 = 10\,\mathrm{K}$, coming from the vacuum tube at $T_2 = 300\,\mathrm{K}$ can be as high as $\dot{Q}_r/A_1 \sim 460\,\mathrm{W/m^2}$. This huge heat flux is not compatible with the cryogenic environment and needs to be reduced by several orders of magnitude.

To limit this huge contribution, we need to reduce the solid angle under which the warm surface is seen by the cold mirror. This is obtained by providing, in the region adjacent to the mirror, cold sections of the vacuum tube, i.e., adding thermal shields (cryotraps) along the part of the vacuum tube near the cryostat hosting the mirror.

The mirror thermal equilibrium is reached when the power extracted by the cooling system is equivalent to that absorbed by the mirror ($\dot{Q}_{\rm abs} = P_{\rm cool}$). If this condition is met, most of the power absorbed by the mirror flows through its suspension wires (a small fraction is lost in radiation), and then is removed by the heat link directly connected to the cooling system. The equilibrium temperature of the mirror $T_{\rm mir}$ can be calculated by the simple analytical model relating it to the temperature of the thermal bath $T_{\rm bath}$ of the cooler via the power flow through the mirror wires:

$$\dot{Q}_{\rm abs} = \frac{4\Sigma_w}{L} < K_{si} > (T_{\rm bath} - T_{\rm mir}) \equiv \frac{1}{Z_{\rm therm}} \Delta T \tag{14.5}$$

with

$$< K_{si} > = \frac{1}{\Delta T} \int_{T_{\rm bath}}^{T_{\rm mir}} K_{si}(T)\, dT \tag{14.6}$$

and where Σ_w is the wire section, L its length and $K_{si}(T)$ is the thermal conductivity of silicon. For a given thermal input $\dot{Q}_{\rm abs}$, the thermal impedance $Z_{\rm therm}$ is the relevant parameter to yield the final temperature of the mirror: this is the quantity which sets the performance of our system and influences the choice of both the material and the geometry of the mirror suspension wire.

In the design of a cryogenic payload (as an example, we show a prototype, developed in Roma, in Fig. 14.15), a few other issues must be considered. First of all, we need to limit the power dissipated in vacuum by the current flowing into the electromagnetic actuator coils used to steer the mirror: a possible solution is the use of superconducting alloys for the coil wires. In fact, despite of the significant decrease of the copper resistivity with temperature, the heat radiated in vacuum can cause a large drift of the mirror temperature because of the lower thermal capacitance of crystals at cryogenic temperatures.

During the commissioning and noise hunting phase, it can happen that we need to access the last stage of suspension for improving the detector performance. This implies that a short cooling (and warm up) time improves the flexibility of the apparatus.

To avoid any possible contamination of the mirror, the KAGRA project has chosen to cool the mirror by embedding the payload in a heavy shield thermally connected to the PT cold heads. Thin wires made of pure aluminum connect the shield to the marionette and the heat is extracted from the suspended elements of the payload both via radiation and solid conduction. This approach eliminates the danger of mirror contamination but implies to wait nearly one month to bring the 23 kg sapphire mirror at 20 K.

In the case of the proposed ET detector, the silicon mirror will have a mass with a thermal capacitance 3–4 times that of the KAGRA mirror: another approach should therefore be considered. In Fig. 14.16, we plot the typical values of the heat exchange coefficients in function of the temperature for various mechanisms of heat transfer.

Fig. 14.15 The first prototype of cryogenic payload built in the VIRGO laboratory of the university of Rome *La Sapienza*. The payload is ready to be inserted in the inner vacuum chamber of the vibration free cryostat equipped with a PT cryocoolers

The plot shows that an improvement of the cooling time is obtained by using a low pressure helium gas, which improve the heat exchange between the cold shield of the cryostat and the payload. The drawback of this solution is a more complex design of the cryostat: it requires to transform the cold shield in a second vacuum chamber hosting the payload. During the cooling phase, the inner chamber is filled with helium gas insuring a more efficient heat extraction. Then, in the low temperature state, the gas is pumped out.[7] This approach implies to solve two problems at least:

- insure the vacuum tightness of the inner vacuum chamber, which contains the payload suspended vertically via a cable to the room temperature super attenuator and which is connected horizontally to the kilometric vacuum tube via the cold traps,

[7] This technique is applied also in the cooling process of all the GW resonant antennas.

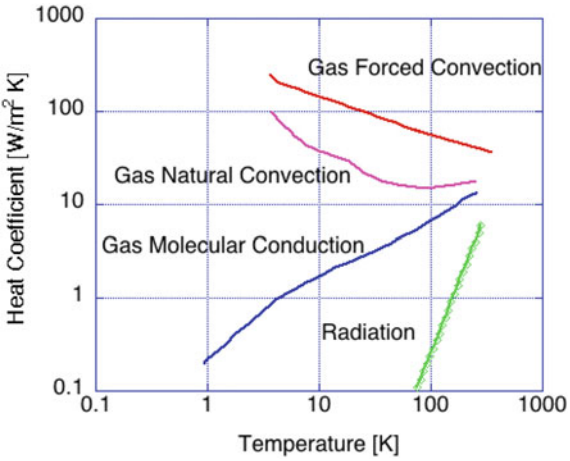

Fig. 14.16 Typical curves of the heat transfer coefficients versus temperature for the various mechanisms of heat exchange. We notice that the radiative exchange is poor, while the gas heat exchange is a way to reduce the cooling time significantly

- limit the high risk of mirror contamination by adding a purification system for the gas flowing in and out the inner vacuum chamber.

Although a few technical solutions have been proposed, at present none of them is yet validated by an experimental test.

14.4 Conclusion

The third generation of GW detectors is renewing the alliance between low temperature physics and gravitational wave astronomy. One of the most challenging goals in the construction of a new generation gravitational wave interferometers is cooling the mirrors at low temperature. Here, we presented the alternative strategies for cooling the mirrors in the case of the Einstein Telescope trying to focus on those aspects which require R&D activity and experimental tests.

At present, the construction of the Japanese detector KAGRA has started. This 3 km-arm interferometer has an innovative design and implements the key technologies of a third generation gravitational wave observatory. The KAGRA project already made few crucial choices to overcome several difficulties associated to the use of cryogenics in a GW interferometer. The common aspects of the KAGRA and ET detectors are pushing for a tighter collaboration between the Japanese and European scientists, and it will influence the final design of the ET cryogenic detector.

References

1. J. Weber, Detection and generation of gravitational waves. Phys. Rev. **117**, 306 (1960)
2. J. Weber, Evidence for discovery of gravitational radiation. Phys. Rev. Lett. **22**, 1320 (1969)
3. M. Lee, D. Gretz, S. Steppel, J. Weber, 1979 Gravitational radiation detector observations in 1973 and 1974. Phys. Rev. **D19**, 893 (1979)

4. J.L. Levine, B. Garwin, New negative results for gravitational wave detection and comparison with reported detector. Phys. Rev. Lett. **33**, 794 (1974)
5. D.H. Douglass, R.O. Gram, J.A. Tyson, R.W. Lee, Two-detector-coincidence search for bursts of gravitational radiation. Phys. Rev. Lett. **35**, 480 (1975)
6. B.W.P. Drever, J. Hough, B. Bland, G.W. Lessnoff, Search for short bursts of gravitational radiation. Nature **246**, 340 (1973)
7. O.D. Aguiar, Res. Astron. Astrophys. **11**, 1–42 (2011)
8. W. Fairbank, The use of low-temperature technology in gravitational wave experiments, in *Proceedings of the International School on Experimental Gravitation* (Italy, Varenna, 1972), p. 280
9. E. Mauceli, Z.K. Geng, W.O. Hamilton, W.W. Johnson, S. Merkowitz, A. Morse, The Allegro gravitational wave detector: data acquisition and analysis. Phys. Rev. D **54**, 1264 (1996)
10. P. Astone, M. Bassan, P. Bonifazi, P. Carelli, M.G. Castellano, G. Cavallari, E. Coccia, C. Cosmelli, V. Fafone, S. Frasca, E. Majorana, I. Modena, G.V. Pallottino, G. Pizzella, P. Rapagnani, F. Ricci, M. Visco, Long-term operation of the Rome "Explorer" cryogenic gravitational wave detector. Phys. Rev. **D47**, 362 (1993)
11. P. Astone, M. Bassan, P. Bonifazi, P. Carelli, E. Coccia, C. Cosmelli, V. Fafone, S. Frasca, A. Marini, G. Mazzitelli, Y. Minenkov, I. Modena, G. Modestino, A. Moleti, G.V. Pallottino, M.A. Papa, G. Pizzella, P. Rapagnani, F. Ricci, F. Ronga, R. Terenzi, M. Visco, L. Votano, Astropart. Phys. **7**, 231 (1997)
12. M. Cerdonio, M Bonaldi, D. Carlesso, E. Cavallini, S. Caruso, A. Colombo, P. Falferi, G. Fontana, P.L. Fortini, R. Mezzena, A. Ortolan, G.A. Prodi, L. Taffarello, G. Vedovato, S. Vitale, J.P. Zendri, The ultracryogenic gravitational-wave detector AURIGA. Class. Quant. Grav. **14**, 1491 (1997)
13. F. Acernese et al., First joint gravitational wave search by the AURIGA EXPLORER NAUTILUS Virgo Collaboration. Class. Quant. Grav. **25**, 205007 (2008)
14. L. Tisza, C. R. Acad. Sci. **207**, 1035, 1186 (1938)
15. F. London, Phys. Rev. **54**, 947 (1938)
16. L.D. Landau, J. Phys. (USSR) **5**, 7 (1941)
17. L.D. Landau, J. Phys. (USSR) **11**, 91 (1947)
18. G. Bon Mardion, G. Claudet, P. Seyfert, Practical data on steady state heat transport in superfluid helium at atmospheric pressure. Cryogenics **19**, 45 (1979)
19. P. Astone, M. Bassan, P. Bonifazi, E. Coccia, C. Cosmelli, Noise behaviour of the EXPLORER gravitational wave antenna during the l transition to superfluid phase. Cryogenics **32**, 668 (1992)
20. P. Puppo, F. Ricci, Cryogenics and Einstein telescope. Gen. Relativ. Gravit. **43**, 657–669 (2011)
21. F. Ricci, Low temperature and future gravitational wave experiments, ed. by J. Dumarchez, J.T.T. Van, in *Proceedings of the XLIInd Rencontres de Moriond, Gravitational Waves and Experimental Gravity*, vol. 177 (The Gioi Publishers, 2007)
22. E.I. Mikulin, A.A. Tarasov, M.P. Shkrebyonock, Low temperature expansion pulse tubes. In *Advances in Cryogenic Engineering*, vol. 29 (Plenum Press, New York, 1984), pp. 629–637
23. S. Zhu, P. Wu, Z. Chen, Double inlet pulse tube refrigerators: an important improvement. Cryogenics **30**, 514 (1990)
24. S. Caparrelli, E. Majorana, V. Moscatelli, E. Pascucci, M. Perciballi, P. Puppo, P. Rapagnani, F. Ricci, Vibration-free cryostat for low-noise applications of a pulse tube cryocooler. Rev. Sci. Instrum. **77**, 095102 (2006)
25. M.V. Plissi, K.A. Strain, Aspects of the suspension system for GEO600. Rev. Sci. Instrum. **69**, 3055 (1998)